

Article

Prospecting Prediction for the Yulong Metallogenic Belt in Tibet Based on Remote Sensing Alteration Information and Structural Interpretation

Yilin Feng ¹, Jingjing Dai ^{2,3,*}, Longyang Bai ² and Changyu Wu ¹

¹ School of Earth Sciences and Resources, China University of Geosciences (Beijing), Beijing 100083, China; 2001220184@email.cugb.edu.cn (Y.F.); 2001210193@email.cugb.edu.cn (C.W.)

² MNR Key Laboratory of Metallogeny and Mineral Assessment, Institute of Mineral Resources, Chinese Academy of Geological Sciences, Beijing 100037, China; bailongyang@cags.ac.cn

³ SinoProbe Laboratory, Chinese Academy of Geological Sciences, Beijing 100094, China

* Correspondence: daijingjing@cags.ac.cn; Tel.: +86-136-5135-7252

Abstract: The Yulong porphyry copper belt in eastern Tibet is located in the middle of Tethys–Himalayan metallogenic mega-province, which is one of the three major porphyry copper metallogenic mega-provinces. The Yulong copper belt belongs to the super porphyry copper belt and represents one of the most important copper mineralization prospecting areas in China. A significant quantity of research data shows that this study area belongs to the environment of intracontinental collision and compression, with a complex geological structure, magmatic rock development and excellent metallogenic geological background. However, because this area is located in an alpine and high-altitude area, it is difficult to carry out any traditional field geological surveys, and the existing studies of both prospecting and prediction are relatively weak. This study focused on information extraction for alteration minerals in the Yulong metallogenic belt and its surroundings based on multispectral data and hyperspectral data, establishing a spectral library of alteration minerals in this area. Based on Sentinel-1A radar data and Landsat-8 OLI color synthesis data, the linear structure of the study area was interpreted. On this basis, the information extraction results relating to alteration minerals obtained from multi-source remote sensing data, linear structure interpretation results and the geochemical exploration data of the study area were superimposed to comprehensively analyze the metallogenic geological conditions and mineralization characteristics in the area, establish remote sensing prospecting indicators there and optimize the potential areas for prospecting, providing technical support for the next step of prospecting and exploration in the area.



Citation: Feng, Y.; Dai, J.; Bai, L.; Wu, C. Prospecting Prediction for the Yulong Metallogenic Belt in Tibet Based on Remote Sensing Alteration Information and Structural Interpretation. *Remote Sens.* **2024**, *16*, 1343. <https://doi.org/10.3390/rs16081343>

Academic Editor: Richard Gloaguen

Received: 13 March 2024

Revised: 5 April 2024

Accepted: 8 April 2024

Published: 11 April 2024



Copyright: © 2024 by the authors. Licensee MDPI, Basel, Switzerland. This article is an open access article distributed under the terms and conditions of the Creative Commons Attribution (CC BY) license (<https://creativecommons.org/licenses/by/4.0/>).

1. Introduction

The alteration in surrounding rock is an important characteristic of the mineralization of hydrothermal deposits, and it also provides a very effective indication of prospecting [1]. In recent years, satellite remote sensing technology, with its advantages of a short cycle, low cost, low risk and green environmental protection, has played an important role in the extraction of altered mineral information in hydrothermal deposits. At present, Landsat-8 OLI, ASTER and other multispectral data have been widely used in the extraction of altered mineral information, which then provides an important reference for the delineation of potential areas for prospecting [2–4]. However, due to the restrictions in spectral resolution, the extraction accuracy of the precise alteration type needs to be further improved. The hyperspectral data have the characteristics of a combination of an atlas, a large number of bands and narrow width, which greatly improve the precision and accuracy of rock and mineral identification [5–9]. However, due to the high cost of hyperspectral data, the

narrow scanning width and being prone to be affected by water vapor absorption bands, the current research on hyperspectral alteration mineral mapping has mainly focused on the extraction of typical hydroxyl and carbonate minerals in the short-wave infrared band [10,11]. Therefore, the combination of multispectral and hyperspectral data can effectively improve the reliability of information extraction of altered minerals.

The Yulong porphyry copper belt in Tibet, located at the southeast margin of the Qinghai-Tibet Plateau, is not only an important metallogenic prospecting zone in China, but also provides one of the most abundant copper resources in China [12,13]. It is over 400 km in length and about 30~70 km in width, which consists of one giant copper deposit (Yulong), two large deposits (Malasongduo, Duoxiasongduo), four medium-sized deposits (Zhanaga, Mangzong, Baomai, Mamupu) and more than twenty small deposits or mineralization points [14,15]. Influenced by the collision and orogeny between the Indian Plate and the Asian Plate, there are numerous Cu, Ag, Pb, Zn, Au and other polymetallic deposits in the region [16]. The types of deposits are mainly porphyry, skarn and epithermal. Since the Triassic period, complex and varied tectonic evolutions and magmatic activity have taken place in the study area, and a NW trending arc tectonic system has been formed through the Indosirian, Yanshanian and Himalayan stages. The complex tectonic movement and frequent magmatic activity provided favorable conditions for the metal mineralization in this area. However, because the study area of the three rivers (Jinsha River, Lancang River, Nujiang River) water system presents as mountain and canyon landforms with an altitude of 3000~5000 m, the natural environment is harsh, and the transportation is very inconvenient, making it difficult to carry out traditional geological work. The existing research has mainly focused on the northern section of the Yulong copper mine, and the deposits found in the southern section are not large in scale. In general, the study area has been the source of a low degree of work but has significant great prospecting potential [17].

Based on Landsat-8 OLI, ASTER multispectral data, GF-5, ZY1-02D hyperspectral data and Sentinel-1A radar data, this paper takes the Yulong porphyry copper belt in Tibet, which is poorly studied and has great ore-forming potential, as its study area to extract information from the multi-source remote sensing data and carry out structural interpretation. Finally, multi-element information such as remote sensing alteration information extraction, structural interpretation and geochemical exploration is comprehensively superimposed to analyze the regional metallogenic prospect area, so as to provide technical support for follow-up mineral exploration in the study area.

2. Geological Setting of Yulong Porphyry Copper Belt

The current study area is located in the eastern part of the Tibet Autonomous Region, in the middle of the Sanjiang tectonic belt in the eastern section of the Tethys tectonic domain. The tectonic line changed from near NW-SE to near NS rapidly (Figure 1), and the tectonic position is unique. The outcrop strata in this area are mainly Paleozoic: Lower Ordovician, Devonian, Lower Carboniferous, Permian; Mesozoic: Triassic; and Cenozoic: Paleogene [18]. Controlled by a series of NNW trending faults and strike-slip pull-apart basins, the Yulong porphyritic copper belt is composed of four secondary structural units, from west to east: Tuoba anticline, Yulong syncline, Qingnidong-Haitong uplift and Tertiary Gongjue basin. There is a Ziga fault zone in the east and the Tuoba-Mangkang fault belt in the west, among which there is the Jueyong fault (also known as the Wenquan fault [19]). It has been discovered that the anticlinal structure of the series of secondary fold development between the uplift zone and the syncline is of great significance to the diagenesis and mineralization of the porphyry copper deposits, and is often the production site of porphyry copper deposits (spots) in this belt [12].

Influenced by the evolution of the Tethys structure, the magmatic activity in the study area is manifested from Hercynian to Himalayan, and the southern section is more intense than the northern section. The eruptive activities include the neutral and the middle basic volcanic rocks of the late Hercynian Permian and the medium and acidic volcanic lava of the calc-alkaline series formed by the early Indosinian (Lower Triassic) orogeny. The

intrusive activities started in the Indosinian and continued to the Himalayan stage and were characterized by the formation of a large number of medium and acidic epipelagic porphyritic intrusions [12]. Among these intrusions, the ore-bearing porphyry bodies closely related to mineralization are concentrated in the Triassic and the lower strata, including the Lower Triassic Malasongduo Formation (T_1m), Upper Triassic Jiapila Formation (T_3j) and Bolila Formation (T_3b) [13]. Therefore, the favorable regional tectonic geological background and the metallogenic conditions promote the formation and enrichment of the polymetallic minerals in the metallogenic belt.

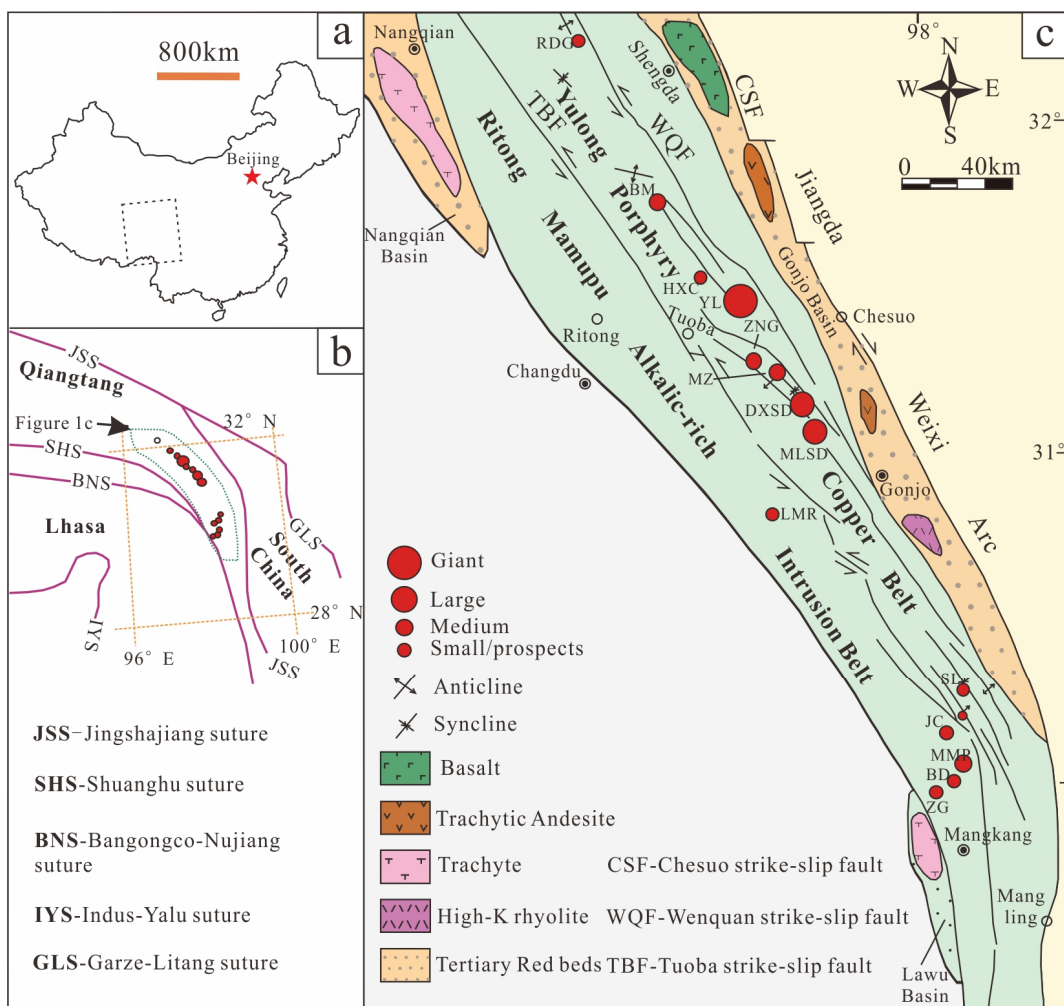


Figure 1. (a) Geographical location of the Yulong metallogenic belt; (b) geotectonic location of the Yulong metallogenic belt; (c) geological map of the Yulong metallogenic belt. Deposits names (from north to south): RDG—Ridanguo; BM—Baomai; HXC—Hengxingcuo; YL—Yulong; ZNG—Zhanaga; MZ—Mangzong; DXSD—Duoxiasongduo; MLSD—Malasongduo; SL—Seli; JC—Jicuo; MMP—Mamupu; BD—Bada; ZG—Zongguo. (reprinted from Ref. [14]. 2018, Lin, B.; Wang, L.Q.; Tang, J.X.; Song, Y.; Cao, H.W.; Baker, M.J.; Zhang, L.J.).

3. Materials and Methods

3.1. Remote Sensing Data and Preprocessing

3.1.1. Landsat-8 and ASTER

Landsat-8, the eighth satellite in the United States Landsat program, was launched on 11 February 2013 aboard an Atlas-V rocket. The satellite carries an operational land imager (OLI) and a thermal infrared sensor (TIRS). Among them, the OLI sensor mainly consists of nine spectral bands, including one panchromatic band with a spatial resolution of 15 m and eight visible-near-infrared (VNIR) and short-wave infrared (SWIR) bands with a spatial

resolution of 30 m (Table 1). Compared with an ETM+ sensor, it has an increased spectral range and signal-to-noise ratio and has better advantages in the extraction of alteration information [20].

Table 1. The characteristic parameters of Landsat-8 OLI and ASTER multispectral data.

Landsat-8 OLI			ASTER		
Wave Band	Wavelength/ μm	Spatial Resolution/m	Wave Band	Wavelength/ μm	Spatial Resolution/m
Band1 Coastal	0.43–0.45	30			
Band2 Blue	0.45–0.51	30			
Band3 Green	0.53–0.59	30	Band1 Green	0.52–0.60	15
Band4 Red	0.64–0.67	30	Band2 Red	0.63–0.69	15
Band5 NIR	0.85–0.88	30	Band3N NIR	0.78–0.86	15
			Band3B	0.78–0.86	15
Band6 SWIR1	1.58–1.65	30	Band4 SWIR1	1.60–1.70	30
Band7 SWIR2	2.11–2.29	30	Band5 SWIR2	2.145–2.185	30
			Band6 SWIR3	2.185–2.225	30
Band8 Pan	0.50–0.68	15	Band7 SWIR4	2.235–2.285	30
Band9 Cirrus	1.36–1.38	30	Band8 SWIR5	2.295–2.365	30
			Band9 SWIR6	2.360–2.430	30

ASTER is an advanced optical sensor that was successfully launched aboard the Japanese Terra satellite on 18 December 1999 and began collecting data in 2000. It contains a total of 14 spectral channels from visible-near-infrared to thermal infrared (Table 1), with spatial resolutions ranging from 15 m to 90 m. It is worth noting that since 1 April 2008, ASTER's detector on the SWIR bands cannot be used normally due to high temperatures, so it is necessary to pay attention to the imaging time during the data selection process.

Seven scenes of Landsat-8 data and thirty scenes of ASTER were selected for this study. The image quality was generally good, and, in essence, there was no cloud cover. With the inclusion of a small amount of vegetation or snow cover, the complete coverage of the study area could be achieved. The preprocessing procedure for the Landsat-8 and ASTER multispectral data is essentially the same and mainly includes radiometric calibration, atmospheric correction and masking.

3.1.2. GF-5 and ZY1-02D

The GF-5 satellite was successfully launched on 9 May 2018. It is the first full-spectrum satellite in the world to achieve the comprehensive observation of both the atmosphere and land and is also an important remote sensing satellite in China's high-resolution Earth observation system. This satellite carries six types of sensors to acquire data in the ultraviolet to long-wave-infrared range. Its visible short-wave-infrared hyperspectral camera (AHSI) has a total of 330 bands of VNIR-SWIR, and can obtain hyperspectral data with a width of 60 km and a spatial resolution of better than 30 m. The specific parameters of the GF-5 are shown in Table 2. Compared with other hyperspectral data, these data have the advantages of high spatial spectral resolution and a large number of bands, and they are more conducive to the extraction of information concerning altered minerals [21].

Table 2. The characteristic parameters of GF-5 and ZY1-02D hyperspectral data.

Satellite Sensor	GF-5 AHSI	ZY1-02D AHSI
Spectral range/ μm	0.45–2.5	
Number of spectral channels	330	166
Spectral resolution (VNIR)/nm	5	10
Spectral resolution (SWIR)/nm	10	20
Spatial resolution/m	30	30
Width/km	60	60

The ZY1-02D is the first civil hyperspectral satellite independently built and successfully operated by China, which was launched on 12 September 2019. The hyperspectral camera (AHSI) carried by the satellite can obtain hyperspectral data with a width of 60 km and a spatial resolution of better than 30 m. The specific parameters are shown in Table 2. Compared with GF-5, ZY1-02D data are much lower in spectral channel number and spectral resolution; however, the data have the advantages of low noise information, high signal-to-noise ratio and clarity. They also have great application potential in the field of information extraction of altered minerals.

Due to the limited coverage of high-quality GF-5 data in the study area, this study mainly used GF-5 data which were supplemented with ZY1-02D data to extract the information concerning altered minerals in the study area. In this study, 14 scenes of GF-5 data and 23 scenes of ZY1-02D data were selected for the detailed identification of altered minerals; the image quality was generally good, with almost no cloud cover, and complete coverage of the study area could be achieved with a small amount of vegetation or snow cover. Unlike multi-spectral data preprocessing, hyperspectral data also requires band selection to exclude the influence of overlapping bands and water vapor absorption bands of VNIR and SWIR sensors. The preprocessing of GF-5 and ZY1-02D hyperspectral data is essentially the same, both based on ENVI 5.3 platform, which mainly includes band selection, bad line repairs and stripe removal, radiometric calibration, atmospheric correction, spectral smoothing and interference masking.

3.1.3. Sentinel-1

Sentinel-1 is an earth observation satellite from the European Space Agency's Copernicus Program (GMES). It consists of two polar-orbiting satellites, A and B, in the same orbital plane, which were successfully launched on 3 April 2014 and 25 April 2016, respectively. The satellites are equipped with C-band synthetic aperture radar with SM, IW, EW and WV 4 types of imaging modes.

Seven scenes of Sentinel-1A ground-range-detected (GRD) data were selected for this study; the imaging mode is interference wide-field mode (IW), and the polarization mode is VV and VH polarization. The image quality was generally good, and the study area could be completely covered by the images. The preprocessing of Sentinel-1A data was based on the SNAP platform, including orbit correction, thermal noise removal, radiometric calibration, filtering, terrain correction and decibel processing.

3.2. Alteration Information Extraction

3.2.1. Multispectral Mineralization Alteration Anomaly Extraction

The extraction of mineralization alteration information from multispectral images was mainly conducted based on the method of principal component analysis (PCA). The PCA, as one of the common methods of extracting alteration information of remote sensing, is characterized by undemanding quality of atmospheric correction images, easy realization and being effective and steady and is widely used by geologists [22–24]. Its essence is the compression of the number of remote sensing variables in multispectral information through orthogonal transformation, and the concentration of useful information into new components, as far as possible. Each component is unrelated to the others, thus providing highlights of specific geological content [25,26]. As there is a different spectral response mechanism to the radicals and ions of each mineral, the recognition ability in relation to each mineral is also different. Combined with the spectral response mechanism of typical altered minerals in visible-near-infrared and short-wave infrared (VNIR–SWIR) spectra, this indicates that iron-stained alteration minerals take on some diagnostic features in the VNIR (0.4~1.3 μm) band (Figure 2a), while the hydroxyl alteration minerals present some diagnostic features in the SWIR (1.3~2.5 μm) band (Figure 2b).

As can be seen from Table 1, the ASTER data have six bands in SWIR, which is suitable for extracting the alteration information of hydroxyl minerals and clay minerals that possess strong absorption spectra in the SWIR band. While ASTER has only three bands in the

VNIR, Landsat-8 OLI has five bands in VNIR, which can therefore provide more abundant spectral information [27]. Therefore, OLI2, OLI4, OLI5 and OLI6 of the Landsat-8 data were selected to extract the information relating to iron-stained alteration minerals for each scene, while the ASTER1, ASTER3, ASTER4 and ASTER6 (ASTER8) of the ASTER data were selected to extract the information of hydroxyl alteration minerals for each scene. Combined with the spectral characteristics of typical minerals, the selection criterion for the principal component representing the iron-stained anomaly is that the OLI2 and OLI5 coefficient symbols are opposite; therefore, PC4 is selected as the iron-stained anomaly component (Table 3). The selection criterion for the principal component representing the hydroxyl anomaly is that the ASTER1 and ASTER4 coefficient symbols are identical and the ASTER3 and ASTER6 (ASTER8) coefficient symbols are opposite, so PC4 is selected as the hydroxyl-anomaly component (Table 4).

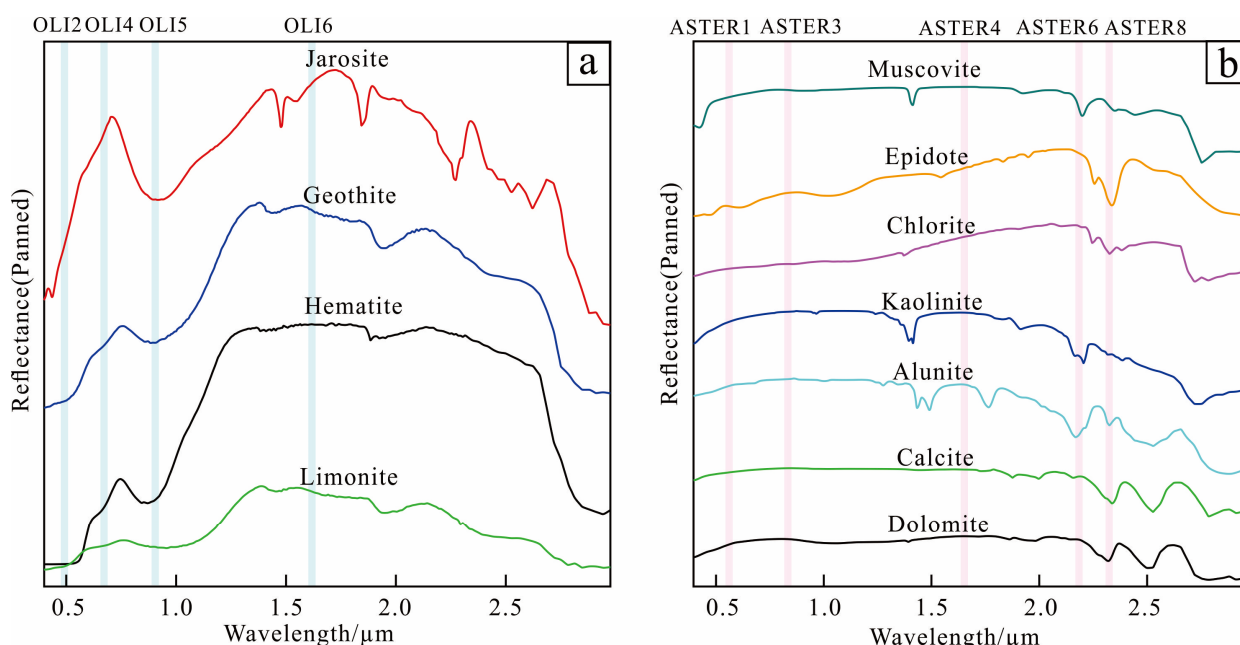


Figure 2. Spectral curves of typical minerals (according to the USGS): (a) typical iron-stained alteration mineral spectra; (b) typical argillic alteration mineral spectra.

Table 3. Statistical results of iron-stained minerals with OLI2, 4, 5 and 6 (take the statistical results of one scene data as an example).

Eigenvectors	OLI2	OLI4	OLI5	OLI6
PC1	0.144101	0.335882	0.496055	0.787622
PC2	0.398654	0.589867	0.400577	-0.576775
PC3	0.488158	0.390769	-0.749814	0.216288
PC4	0.762897	-0.621723	0.176765	0.014228

Table 4. Statistical results of hydroxyl minerals with ASTER1, 3, 4 and 6 (8) (take the statistical results of one scene data as an example).

Eigenvectors	ASTER1	ASTER3	ASTER4	ASTER6
PC1	0.209560	0.397973	0.232984	0.511177
PC2	0.766223	0.499220	-0.354752	-0.194506
PC3	0.561645	-0.733563	-0.028445	0.381615
PC4	-0.231392	0.232984	-0.580467	0.745141

Table 4. Cont.

Eigenvectors	ASTER1	ASTER3	ASTER4	ASTER8
PC1	0.229429	0.419489	0.750621	0.456025
PC2	0.766392	0.466710	-0.426878	-0.112250
PC3	0.479851	-0.715509	-0.053543	0.504900
PC4	-0.360207	0.307014	-0.501474	0.724236

3.2.2. Mineral Identification Based on Hyperspectral Data

The essence of the fine identification of hyperspectral minerals is to classify the end-members spectrum and then identify it using different methods in order to achieve the purpose of mineral classification and extraction in the image. Therefore, the fine identification of hyperspectral minerals includes two steps: endmember extraction and alteration mineral mapping.

Hyperspectral data have the characteristics of significant volume and redundant information, so the minimum noise fraction (MNF) was first used to denoise and reduce the dimensions of the preprocessed data, and the useful signal was concentrated in the front band to reduce the correlation between each band. After that, the pure pixels were delineated through calculating the pixel purity index (PPI) and employing N-dimensional visualization tools, and the unknown endmembers were identified with the use of a standard spectrum library or measured spectrum, focusing on comparing the positions of the diagnostic absorption characteristics of various alteration minerals and, finally, determining the spectral curves of typical alteration minerals in the study area (Figure 3).

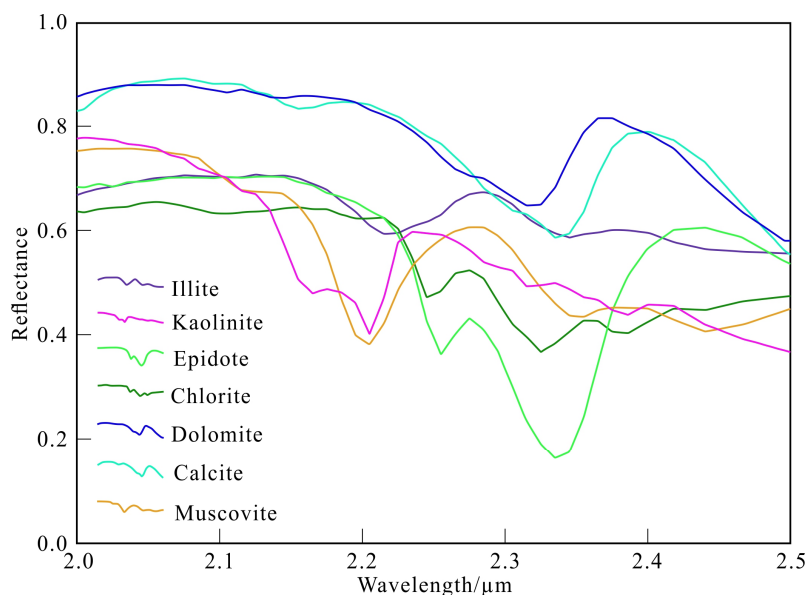


Figure 3. Image endmember spectral curves extracted from GF-5 AHSI.

As a comprehensive method combining linear mixing theory with matched filtering technology [28], mixture-tuned matched filtering (MTMF) has been widely used in hyperspectral mineral mapping and has achieved good results [10,29,30]. MTMF uses the linear spectrum mixing theory and assumes that the content of each endmember in the pixel is positive and the sum is one in order to constrain the feasible mixing results and reduce the probability of false signals. Matching filtering technique is used to maximize the response spectrum of the known endmembers and suppress the mixed unknown background spectrum, so as to match the known spectrum signal. This method can effectively reduce the detection limit of minerals and identify the trace mineral components that are difficult to detect with other methods and is conducive to extracting refined regional alteration mineral information [31].

3.3. Structural Interpretation of Remote Sensing

Since the Triassic, the southwest “Sanjiang” area, where the study area is located, has undergone multiple periods of tectonic–magmatic activity, forming a NW-oriented tectonic system. A series of porphyry–skarn-type deposits formed in the area are mostly controlled by anticline-formed strike-slip structures [17,32]. Therefore, structural interpretation is of great significance for studying the ore-controlling factors in this area and for the further delineation of favorable ore-forming areas. The macroscopic and intuitive nature of remote sensing images provides macroscopic image data for the study of tectonic geomorphology in large areas [33]. In remote sensing images, linear structures are usually displayed indirectly by controlling the local lithology, lithofacies, landform and drainage characteristics, and are manifested in different tones, forms and landforms. Therefore, the interpretation of the linear structure of remote sensing images is mainly achieved from the aspects of tone, morphology and geomorphic development [34].

As an active microwave remote sensing imaging technology, synthetic aperture radar (SAR) possesses unique advantages in the interpretation of information relating to geological structures due to its all-weather image acquisition characteristics and strong penetration capability [35,36]. In this study, the Sentinel-1A data of C-band were selected, which are characterized with rich image structure information, a significant degree of penetration and possess a good detection effect for geological body morphology. Therefore, the data can penetrate clouds and vegetation and reveal information to a certain depth underground, which makes the data very suitable for the identification of geological structures in a certain covered area. In addition, the fracture area is generally accompanied by a certain degree of dislocation phenomena, so that the radar image shows linear information. Specifically, the microwave emitted by the radar transmitter generates echoes in both the rock layer and the fault layer. The rock layer generates stronger echoes due to its uniform and dense texture, while the fault layer significantly weakens the echoes due to the partial absorption of the radar waves and thus appears as a linear structure in the image. In order to make full use of the characteristics of Sentinel-1A radar data, this study carried out image enhancement processing on the preprocessed Level 1 GRD data, that is, color synthesis processing on the basis of band operation of VV and VH polarization data (Figure 4a). The structure information can then be displayed more intuitively.

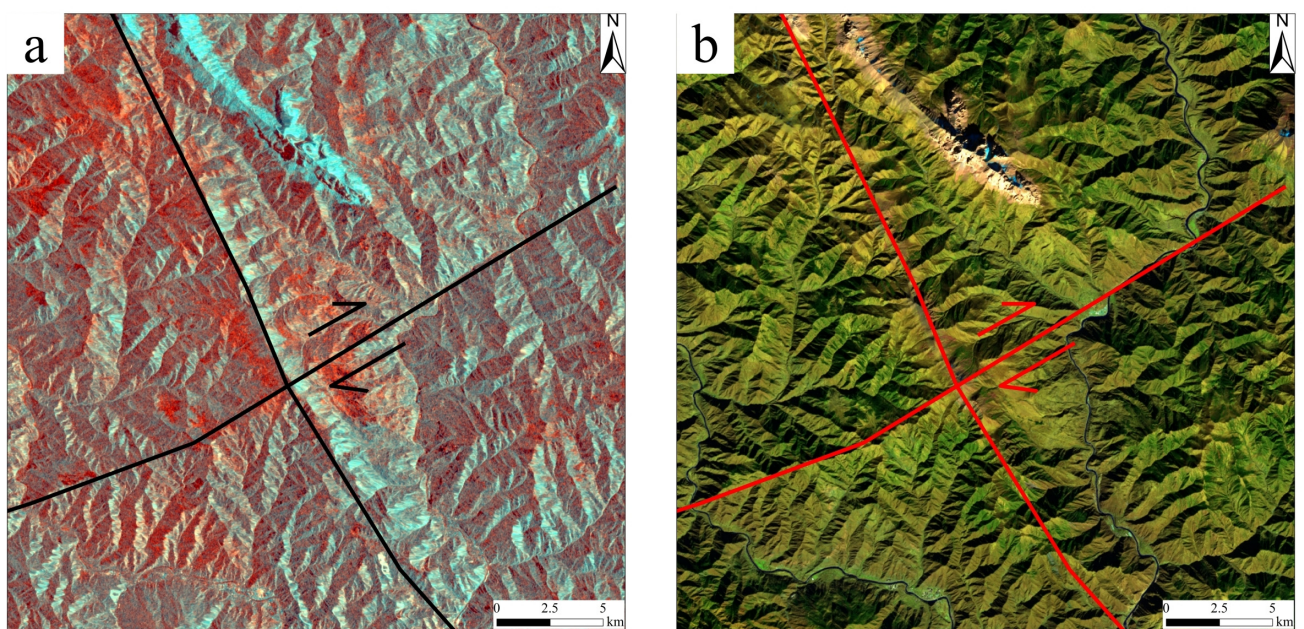


Figure 4. The partial structural interpretation of the study area: (a) Sentinel-1A VV-VH, VV, VV+VH color synthesis; (b) Landsat-8 OLI7, OLI5, OLI2 color synthesis.

At the same time, due to the differences in the spectral response characteristics of the geologic bodies on both sides of the fault and the unique spectral response characteristics of the linear structure itself, there are often obvious tone differences in the optical remote sensing images. Therefore, the false-color composite images of OLI7, OLI5 and OLI2 bands with the low correlation of Landsat-8 (Figure 4b) were used to construct an interpretation of the study area, and various data results were mutually supportive in ensuring the accuracy of the interpretation results.

4. Results

4.1. Alteration Anomaly Extraction

The alteration phenomenon in surrounding rock is an important indicator of the mineralization of hydrothermal deposits. The extraction of that alteration information using remote sensing data can effectively reduce the costs of prospecting, especially in the alpine and high-altitude areas, with few people in the area. In recent years, remote sensing technology has played an important role in the identification of minerals, geological mapping, alteration anomaly zoning, prospecting prediction and other fields [37–41]. However, remote sensing data are easily affected by artificial ground objects, vegetation and other factors, and using a single data source risks the production of significant errors, which leads to failure in meeting the needs of practical work. Therefore, this paper extracts its alteration mineral information based on multi-source remote sensing data. Firstly, the advantages of the Landsat-8 and ASTER multispectral data in VNIR and SWIR spectral ranges were fully utilized, and the alteration information of the iron-stained and hydroxyl groups was extracted via PCA. On this basis, seven typical alteration minerals, including illite, kaolinite, epidote, chlorite, dolomite, calcite and muscovite, were extracted using MTMF based on GF-5 and ZY1-02D hyperspectral data. The results showed that the hydroxyl alteration anomaly information extracted based on the ASTER multispectral data was fundamentally consistent with the typical alteration mineral distribution that was extracted based on hyperspectral data (Figure 5). This proved the reliability of the results. The areas with strong iron-stained alteration anomalies extracted based on Landsat-8, hydroxyl anomalies extracted based on ASTER and typical alteration mineral distribution extracted based on hyperspectral data will be the key areas delineated in the next planned prospecting area.

4.2. Structural Interpretation Results

A large number of studies have shown that the ore types in the present study area are mainly porphyry-skarn deposits. In addition, the widely developed linear structures in the area provide important channels and sites for the emplacement of porphyry and the migration of ore-forming fluids. The linear structure density is an intuitive expression of the linear structural complexity. Structural intensity analyses of the linear structures in the region were carried out. As the study area is located in the eastern part of Tibet, affected by the uplift of the Tibetan Plateau, linear structures are extremely developed in the region, and there are extensive areas with medium and high structural intensity (Figure 6). Based on the known geological and mineral information, it was found that the distribution of Cu, Au and polymetallic ores is essentially consistent with the linear structure trend, and most of them are concentrated in the middle and high value areas of structural density, which indicates that the linear structure in this area is closely related to mineralization, and the middle and high value areas of the linear structure could be some of the key areas to be included in the future planned prospecting area.

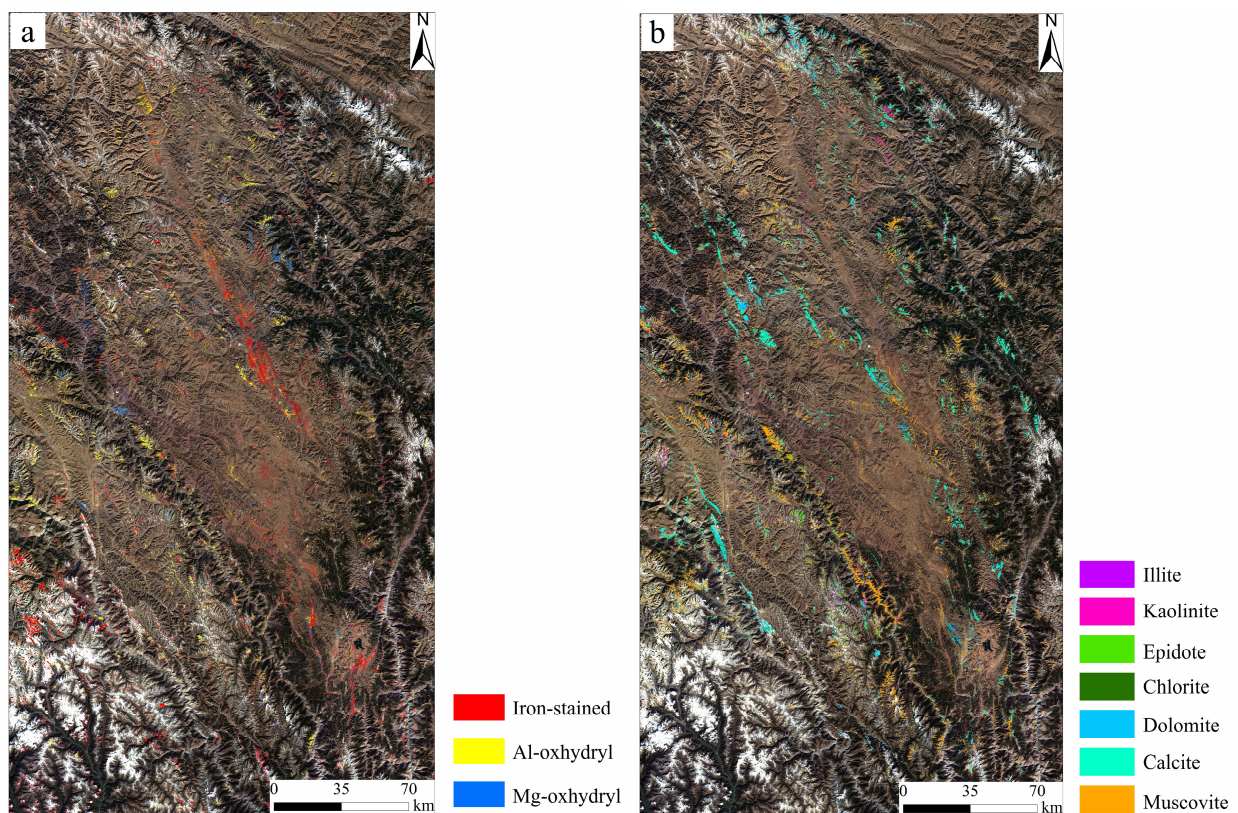


Figure 5. Results of alteration information extraction: (a) multispectral alteration information extraction results; (b) hyperspectral alteration information extraction results.

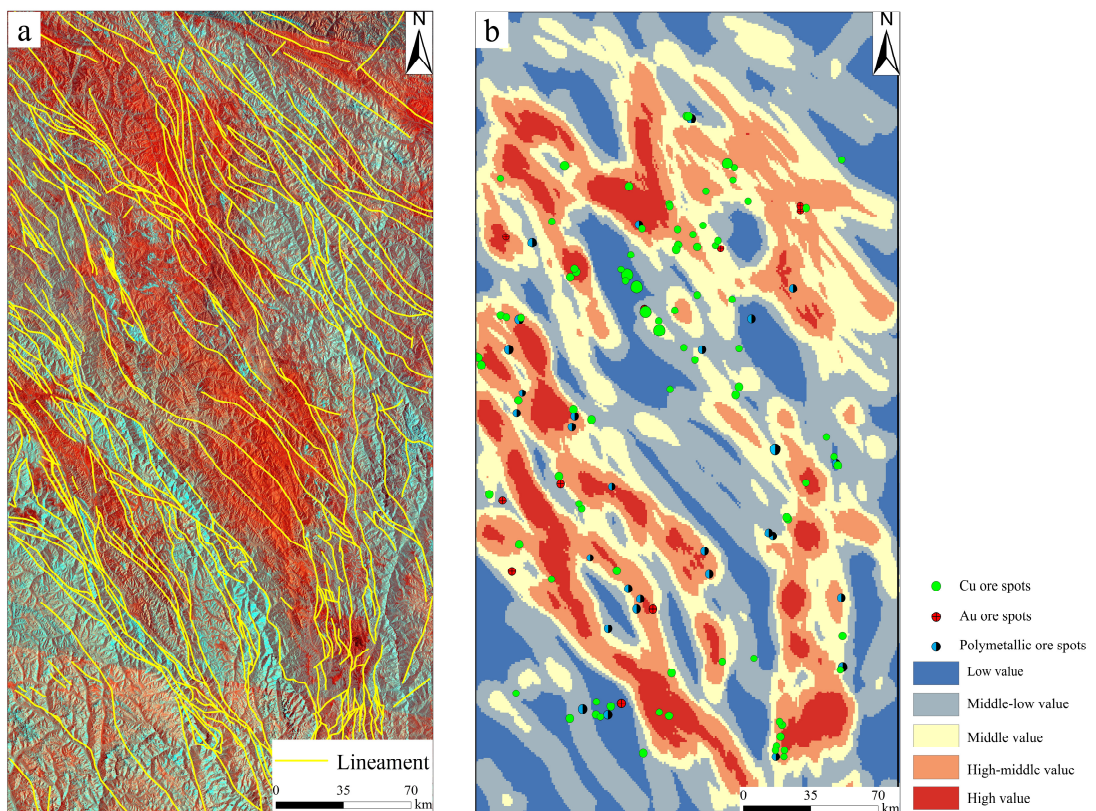


Figure 6. Results of structural interpretation: (a) results of linear structural interpretation; (b) results of linear structural intensity.

4.3. Comprehensive Analysis of Multiple Information and Optimization of Planned Prospecting Area

Mineral exploration is a process of constantly obtaining prospecting information and reducing prospecting risk. In geological prospecting work, any type of information has its value [42]. The use of remote sensing alteration anomaly information is often affected by many factors, so it can be difficult to meet the needs of practical application. Geochemical exploration data provide a type of exploration method that provides direct prospecting opportunities and have a positive effect on solid mineral exploration [42]. Therefore, the superposition of remote sensing, geological, geochemical and other information for multivariate data integration and comprehensive analysis can make up for the shortcomings of a single geological data source in mineral exploration, so as to effectively improve the efficiency of prospecting [36]. This study makes full use of remote sensing alteration mineral information, remote sensing structural information, geological and mineral information and geochemical exploration information to integrate and provide a comprehensive analysis of multiple sources based on ArcGIS 10.6, thereby optimizing potential areas for prospecting. The comprehensive analysis of all types of information and known Cu, Au and polymetallic ore spot information shows that the distribution of alteration minerals on the whole is near the NNW direction, which is, in essence, consistent with the spatial distribution trends of regional, large-linear structures; the geochemical anomalies of Cu and Au elements; and known ore spots (Figure 7). It is a key area for Cu and Au mineral exploration and has significant prospecting potential near the coincidence area where remote sensing alteration is abnormally strong, Cu and Au geochemical values are high, and the linear structure is dense. Therefore, the delineation of potential prospecting areas was carried out based on ArcGIS (Figure 8).

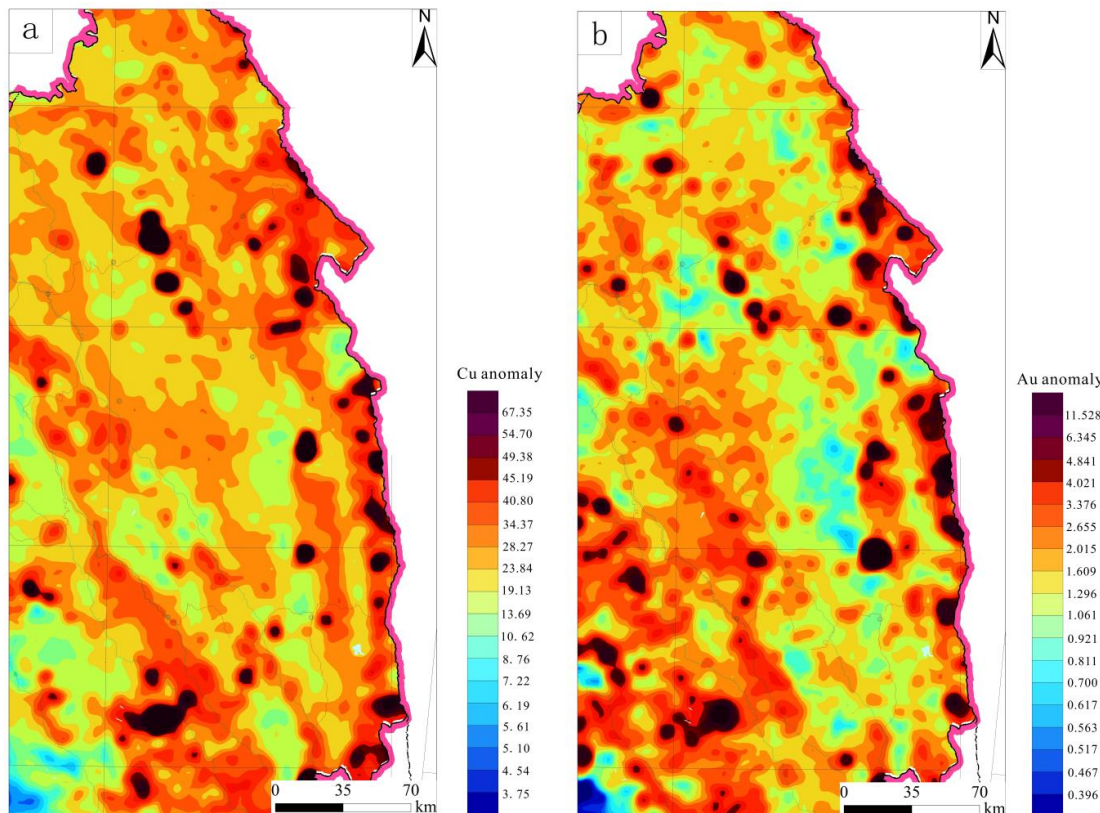


Figure 7. Geochemical anomalies in the study area: (a) Cu anomaly in the study area; (b) Au anomaly in the study area.

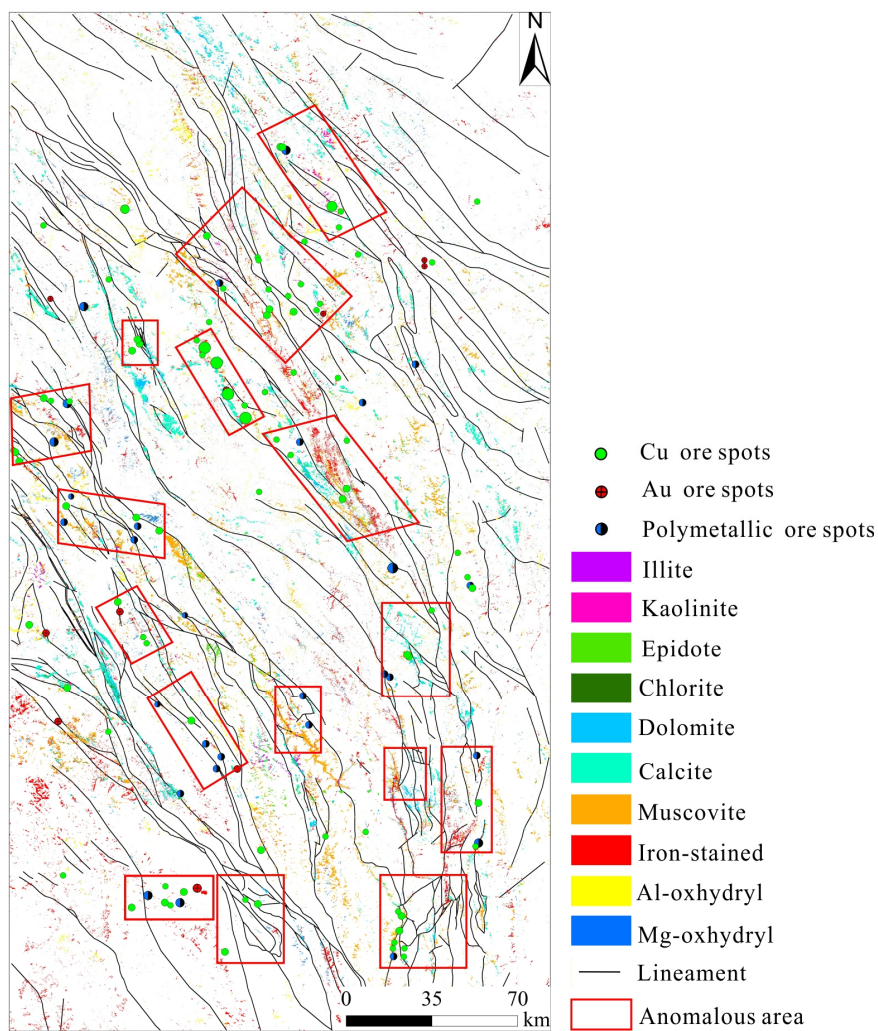


Figure 8. The results of the categorization of the regional multisource information integrated anomaly areas using circles.

5. Discussion

The superposition analysis of the Landsat-8 and ASTER multispectral data and the alteration information extraction results of GF-5 and ZY1-02D hyperspectral data show that there are large areas of vigorous iron-stained and hydroxyl alterations in the Yulong metallogenic belt, and their spatial distribution trend is fundamentally the same. According to the extraction results of the hyperspectral data, the main alterations in the surrounding rock in the study area are sericite and carbonate. The local development of a small amount of chlorite and epidote closely related to mineralization corresponds to the propyl zone in the classical alteration zonation model of porphyry deposits, thus indicating that the mineralization in this area is dominated by medium-low temperature hydrothermal contact metasomatic metamorphism. The mineralization also has typical porphyry deposit alteration characteristics [43]. Combined with the unique geological background of the study area, it is inferred that the porphyry–skarn-type deposits in this area have great metallogenic potential. Previous studies have shown that the northern section of the Yulong metallogenic belt is predominantly porphyry deposits on a large formation scale. The southern section is predominantly skarn deposits that are small in scale. On this basis, combined with the existing characteristics of the porphyry copper polymetallic deposits in the metallogenic belt—“skarn in the upper part and porphyry in the lower part”—it indicates that the denudation in the southern area of the Yulong metallogenic belt is relatively shallow, and the research degree is low. The exploration of the deep, concealed porphyry

copper polymetallic ore body is also one of the key directions for the follow-up prospecting work that takes place in the region.

There were multiple periods of magmatic activity that developed from Hercynian to Himalayan in the study area and were more intense in the southern section than the northern section, forming a series of Eocene porphyry groups spreading in the NW–SE direction [12]. The lithology of porphyry varies regularly in the region, and the silica content increases gradually from north to south. Ivernite dominates the area from Xiariguo to Yulong in the northern section; meanwhile, in the southern section, the area from Jicuo to Mamupu is dominated by syenite and granite porphyry. Combined with the geochemical exploration results of Cu and Au elements, it was found that the type and intensity of metal mineralization also show regular spatial changes with the change in porphyry lithology, and the copper and molybdenum mineralization gradually weaken from north to south, while the gold polymetallic mineralization gradually increases.

The study area is located in the eastern part of the Qinghai–Tibet Plateau and the middle of the Sanjiang River Basin, which belongs to the alpine canyon area of eastern Tibet. Its special tectonic location and intracontinental collision orogeny make the geological structure of this area complex, with the development of linear and arc-shaped structures. Using remote sensing imagery for linear structural interpretation makes the most of the advantages it offers, such as wide area coverage, revealing structural traces on different length scales, and an objective and comprehensive view of the mutual relations and generation sequences of each structural trace. Through the interpretation of the linear structure in the study area, it was discovered that a NW, NNW linear structure has developed in the region, and the arc protrudes in the direction of the NE. Based on the analysis of linear structural density, it was discovered that there were obvious spatial differences in the linear structural intensity on both sides of the large structural belt in the NW direction in the region; that is, there are more medium-high value areas of linear structural intensity on the southwest side, but there are relatively few medium-high value areas of linear structural intensity on the northeast side. By superimposing with the known mineral-site information, it indicates that the structure not only controls the distribution and production state of any intrusion, but also provides channels and places for the migration of ore-forming fluids and the accumulation of ore-forming materials and occupies a dominant position in the whole mineralization process. Therefore, the analysis of the corresponding relationship between tectonic distribution and mineralization alteration has very important theoretical significance for remote sensing in prospecting.

Based on the ArcGIS platform, remote sensing alteration anomaly information, interpretation analysis results of remote sensing geological structures and geochemical exploration data were superimposed on the geological map. It was found that the remote sensing and the geochemical-anomaly information in the study area were generally distributed near the NW along the regional structural framework, indicating that the mineralization in the region was obviously controlled by the main linear structure, in particular, calcite, chlorite, epidote and other alteration minerals with hydroxyl characteristics. It demonstrates that linear structures provide important channels and locations for the migration of hydrothermal fluids and the emplacement of porphyry. In the process of migration and mineralization, hydrothermal fluids often interact with the surrounding rocks to form a series of altered mineral information via remote sensing technology to guide ore exploration. Based on the results of multivariate data analysis, it can be said that this area possesses the development of alteration minerals, a significant alteration of the surrounding rock, the development of linear structures and obvious geochemical anomalies, while the prospecting potential is good and the resource potential is very significant; therefore, it is a favorable area to search for the copper–gold polymetallic deposits that are related to porphyry and skarn.

In order to further confirm the validity and feasibility of the results, the Secuo skarn copper deposit in the southern part of the Yulong metallogenic belt was selected as the key anomalous area for field verification. The field verification results show that the alteration anomaly information extracted from remote sensing data is essentially consistent with the

alteration minerals found in the field. Among them, the alteration information extraction results of the multispectral and hyperspectral data are in good agreement with the known mineral deposit information (Figure 9a,b). Significant iron-stained and mica alterations are detected to the west of the Secuo copper deposit, and carbonate rocks are developed to the southeast of the Secuo copper deposit. We randomly set 58 sampling points in an anomaly area of nearly seven square kilometers for field verification. The results show that the overall coincidence precision reached 86.2%. Calcite, dolomite, illite and muscovite extracted from the images were found in the field. However, some epidote and kaolinite minerals detected by field samples were not extracted from remote sensing images, which requires further research work. We speculate that it might be limited by the spatial resolution of the sensor. According to the field verification results, the west side of the Secuo deposit is the Zhamo pluton, with large-scale limonization on the surface of the pluton (Figure 9c) and sericitization inside (Figure 9d). It is suggested that the rock mass may intrude from west to east and from porphyry–skarn deposits in the Secuo copper deposit (Figure 9e,f). At present, a skarn deposit has been found on the surface. According to the metallogenetic system theory of porphyry–skarn deposits, large-scale porphyry deposits may exist on the west side of the Secuo copper deposit and in its depths; therefore, this can be used as the key region for further prospecting work in this area [44]. The field results show that the integrated prospecting method using optical remote sensing data, radar data and other remote sensing data has important guiding significance for further prospecting and exploration in this area in the future.

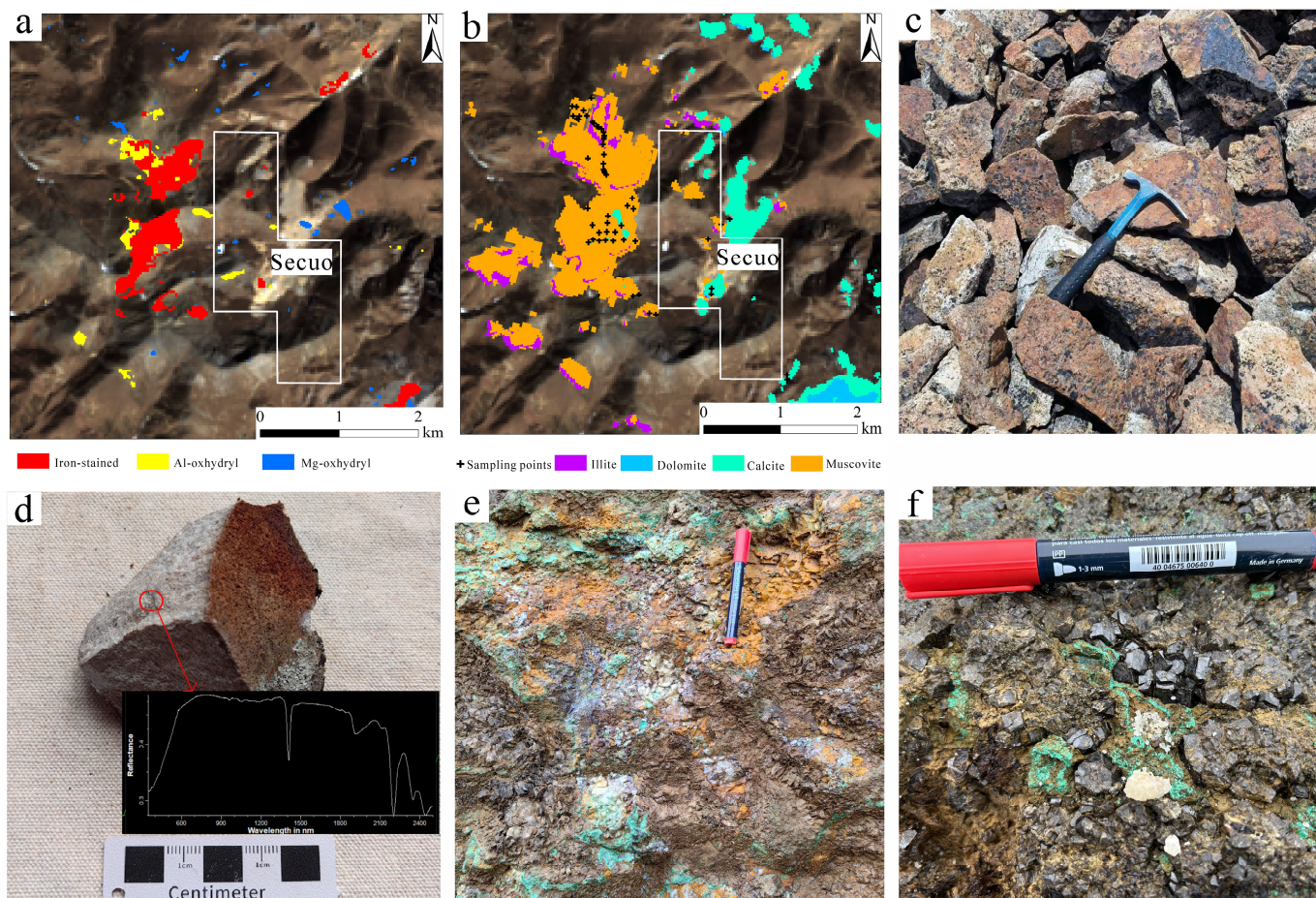


Figure 9. Field verification: (a) the result of multispectral alteration information extraction in the regions validated; (b) the result of hyperspectral alteration information extraction in the regions validated; (c) the region of iron-stained mineralization in the field; (d) the region of muscovite formation in the iron-stained mineralization area; (e,f) the field photographs of Secuo skarn deposit.

Based on the above analytical results, it can be found that remote sensing technology, as a new green exploration methodology, has its unique advantages and potential in the mineral exploration work in alpine and high-altitude areas. However, because this technology is still in the process of continuous development and improvement, there are some limitations in the process of its practical application. For example, the common issue of differing spectra for the same object and the same spectra for different objects often leads to a degree of error in the extraction results. In addition, the spatial resolution of hyperspectral data is limited, and spectral unmixing of mixed pixels is also one of the difficult problems faced by the application of remote sensing technology. Therefore, the reliability of remote sensing prospecting can be improved through different levels of ore-controlling factors in combination with the interpretation results of remote sensing structures. However, if we want to further improve the accuracy of remote sensing prospecting work, on the one hand, we can use a deep learning algorithm combined with multiple sources of information such as terrain and geochemistry to select favorable areas. On the other hand, the problem of how to improve the spatial resolution of hyperspectral data while maintaining its spectral resolution advantages remains an urgent question to be solved.

6. Conclusions

In this study, based on Landsat-8, ASTER multispectral data and GF-5, ZY1-02D hyperspectral data, PCA and MTMF were used to extract the alteration information of the Yulong metallogenic belt. The characteristics of the alteration minerals of iron-stained and hydroxyl groups (illite, kaolinite, epidote, chlorite, dolomite, calcite, muscovite) were successfully extracted, and an endmember spectrum database of typical alteration minerals in this area was established. Based on Sentinel-1A radar data and Landsat-8 optical remote sensing data, the linear structure of the shallow vegetated area was interpreted via image enhancement processing such as color synthesis, and the geological structure information of the study area was effectively extracted. On this basis, ArcGIS was used to complete the structural intensity analysis of the study area. Based on the integration and comprehensive analysis of remote sensing, geological and geochemical information, it is discovered that the key areas for mineral exploration are those where the iron-stained and hydroxyl alteration minerals are abnormally abundant, the linear structural density is medium and high, and the Cu and Au geochemical values are high. On this basis, the metallogenic prospect areas were delineated and verified in the field. The results show that the integrated geological prospecting method using optical remote sensing data, radar data and other remote sensing data, has good prospects for application in this shallow coverage area of high altitude and can provide important technical support for the next Cu and Au mineral exploration in this area.

Author Contributions: Conceptualization, Y.F. and J.D.; methodology, Y.F.; software, Y.F. and L.B.; validation: Y.F. and C.W.; formal analysis, L.B. and C.W.; investigation, Y.F. and J.D.; data curation, Y.F. and J.D.; writing—review and editing, Y.F. and J.D.; supervision, L.B. and C.W.; funding acquisition, J.D. All authors have read and agreed to the published version of the manuscript.

Funding: This research was funded by the National Key Research and Development Program of China (2022YFC2905001), the China Geological Survey Project (DD20230054, DD20230033), and the National Natural Science Foundation of China (42172332).

Data Availability Statement: The data that were used are confidential.

Acknowledgments: The authors would like to thank the editors and reviewers, who provided constructive comments and suggestions. Meanwhile, we give special thanks to the data support provided by the EARTHDATA (<http://www.earthdata.nasa.gov/>), Geocloud (<http://geocloud.cgs.gov.cn/>) and Geospatial Data Cloud websites (<http://www.gscloud.cn/>). The data used in the research was accessed on 30 October 2023.

Conflicts of Interest: The authors declare no conflicts of interest.

References

1. Tang, C.; Chen, J.P.; Zhang, R.S.; Pei, Y.R. Alteration from Aster Remote Sensing Data in Ban Nu Metallogenic Belt, Gaize, Tibet. *Remote Sens. Tech. Appl.* **2013**, *28*, 122–128.
2. Pour, A.B.; Park, T.S.; Hong, J.K.; Muslim, A.M.; Läufer, A.; Crispini, A.; Pradhan, B.; Zoheir, B.; Hashim, M.; Hossain, M.S. Landsat-8, Advanced Spaceborne Thermal Emission and Reflection Radiometer, and WorldView-3 Multispectral Satellite Imagery for Prospecting Copper-Gold Mineralization in the Northeastern Inglefield Mobile Belt (IMB), Northwest Greenland. *Remote Sens.* **2019**, *11*, 2430. [[CrossRef](#)]
3. Guha, A.; Saw, A.K.; Mukherjee, A.; Verma, C.B.; Kumar, K.V.; Rao, P.V.N.; Diwakar, P.G. Eigen vector based analysis of Landsat OLI principal components and constrained energy minimization maps for discriminating iron enriched zones in banded iron formation (BIF) in Sidhi, Madhya Pradesh. *Geocarto Int.* **2022**, *37*, 1880–1898. [[CrossRef](#)]
4. Bai, L.Y.; Dai, J.J.; Song, Y.; Liu, Z.B.; Chen, W.; Wang, N.; Wu, C.Y. Predictive Prospecting Using Remote Sensing in a Mountainous Terrestrial Volcanic Area, in Western Bangongco-Nujiang Mineralization Belt, Tibet. *Remote Sens.* **2023**, *15*, 4851. [[CrossRef](#)]
5. Wang, R.S.; Gan, F.P.; Yan, B.K.; Yang, S.M.; Wang, Q.H. Hyperspectral Mineral Mapping and Its Application. *Remote Sens. Nat. Resour.* **2010**, *1*, 1–13.
6. Jain, R.; Sharma, R.U. Airborne hyperspectral data for mineral mapping in southeastern Rajasthan, India. *Int. J. Appl. Earth Obs. Geoinf.* **2019**, *81*, 137–145. [[CrossRef](#)]
7. Dong, X.F.; Gan, F.P.; Li, N.; Yan, B.K.; Zhang, L.; Zhao, J.Q.; Yu, J.C.; Liu, R.Y.; Ma, Y.N. Fine mineral identification of GF-5 hyperspectral image. *Natl. Remote Sens. Bull.* **2020**, *24*, 454–464. [[CrossRef](#)]
8. Dai, J.J.; Zhao, L.X.; Jiang, Q.; Wang, H.Y.; Liu, T.Y. Review of thermal-infrared spectroscopy applied in geological ore exploration. *Acta Geol. Sin.* **2020**, *94*, 2520–2533.
9. Liu, L.; Yin, C.T.; Khail, S.Y.; Hong, J.; Feng, J.L.; Zhang, H.S. Alteration mapping for porphyry Cu targeting in the western Chagai belt, Pakistan Using ZY1-02D spaceborne hyperspectral data. *Econ. Geol.* **2024**, *119*, 331–353. [[CrossRef](#)]
10. Kruse, F.A. Integrated visible and near infrared, shortwave infrared, and longwave infrared (VNIR-SWIR-LWIR), full-range hyperspectral data analysis for geologic mapping. *J. Appl. Remote Sens.* **2015**, *9*, 096005. [[CrossRef](#)]
11. Fu, M.H.; Dai, J.J.; Wang, X.G.; Hu, Z.H.; Peng, B.; Wan, X.; Zhang, Z.X.; Zhao, L.X. A study on the Thermal Infrared Spectroscopy Characteristic of the Skarn Minerals in Zhuxi Tungsten Deposit, Jiangxi Province. *Spectrosc. Spectr. Anal.* **2023**, *43*, 70–77.
12. Zhang, J.S.; Dou, J.; He, Z.W.; Tang, J.X. Analysis of metallogenic regularity in North Tibetan Yulong porphyry copper belt. *Contrib. Geol. Miner. Resour.* **2008**, *3*, 199–203.
13. Qin, Q.; Wang, L.; Zhong, K.H. Geological characteristics of the Yulong porphyry copper mineralization belt in Tibet. *Sichuan Nonferrous Met.* **2013**, *3*, 27–30+40.
14. Lin, B.; Wang, L.Q.; Tang, J.X.; Song, Y.; Cao, H.W.; Baker, M.J.; Zhang, L.J.; Zhou, X. Geology, geochronology, geochemical characteristics and origin of Baomai porphyry Cu (Mo) deposit, Yulong Belt, Tibet. *Ore Geol. Rev.* **2018**, *92*, 186–204. [[CrossRef](#)]
15. Zhang, X.X.; Tang, J.X.; Lin, B.; He, L.; Shao, R.; Wang, Q.; Yan, G.; Wu, Q.; Du, Q.; Zhaxi, P.C.; et al. Mineralogical characteristics of the Mamupu copper polymetallic deposit in the southern section of the Yulong copper belt, Tibet. *Acta Geol. Sin.* **2022**, *96*, 2062–2077.
16. Chen, J.P.; Tang, J.X.; Li, Z.J. Applications of Chaos in Metallogenetic Conditions in the Northern Part of Three-River Area, China. *Geol. Prospect.* **2003**, *3*, 1–4.
17. Tang, J.X.; Wang, Q.; Yang, H.H.; Gao, X.; Zhang, Z.B.; Zou, B. Mineralization, Exploration and Resource Potential of Porphyry-skarn-epithermal Copper Polymetallic Deposits in Tibet. *Acta Geosci. Sin.* **2017**, *38*, 571–613.
18. Yang, H.; Jiang, Q.Y.; Zheng, C.; Luo, W.; Liu, C.H. Technology of Multielement Information Analysis Used for Metallogenic Prediction in Yulong Area of Tibet, China. *Sichuan Build. Mater.* **2015**, *41*, 240–241+246.
19. Hou, Z.Q.; Ma, H.W.; Zaw, K.; Zhang, Y.Q.; Wang, M.J.; Wang, Z.; Pan, G.T.; Tang, R.L. The Himalayan Yulong porphyry copper belt: Product of large-scale strike-slip faulting in the eastern Tibet. *Econ. Geol.* **2003**, *98*, 125–145.
20. Chu, Q.W.; Zhang, H.Q.; Wu, Y.W.; Feng, Z.K.; Chen, B. Application Research of Landsat-8. *Remote Sens. Inf.* **2013**, *28*, 110–114.
21. Lian, C.Q.; Yao, F.J.; Chen, M.H.; Ma, K.Z.; Wang, H.L. The Study on Alteration Information Extraction of GF-5 Hyperspectral Data in Vegetation Coverage Area: A Case study of Yushui Copper Deposit in Guangdong Province. *Geoscience* **2020**, *34*, 680–686.
22. Wu, Z.C.; Ye, F.W.; Guo, F.S.; Liu, W.H.; Li, H.L.; Yang, Y. A Review on Application of Techniques of Principle Component Analysis on Extracting Alteration Information of Remote Sensing. *J. Geo-Inf. Sci.* **2018**, *20*, 1644–1656.
23. Crosta, A.P.; Moore, J.M. Enhancement of Landsat Thematic Mapper imagery of residual soil mapping in SW Minas Gerais State, Brazil: A prospecting case history in Greenstone belt terrain. In Proceedings of the 7th (ERIM) Thematic Conference: Remote Sensing for Exploration Geology, Calgary, AB, Canada, 2–6 October 1989; pp. 1173–1187.
24. Du, X.C.; Lou, D.B.; Zhang, C.Q.; Xu, L.G.; Liu, H.; Fan, Y.L.; Zhang, L.; Hu, J.M.; Li, B. Study on extraction of alteration information from GF-5, Landsat-8 and GF-2 remote sensing data: A case study of Ningnan lead-zinc ore concentration area in Sichuan Province. *Miner. Depos.* **2022**, *41*, 839–858.
25. Zhang, B.; Zhou, J.; Wang, J.N. Analyses of Alteration Mineral Mapping and Mineral Resources Prospecting Using TM or ETM Data. *J. Earth Sci. Environ.* **2008**, *3*, 254–259.
26. Liu, L.; Pu, X.N.; Hong, J.; Zhang, H.S.; Yasir, S.K. Alteration information extraction and ore-prospecting prediction using ASTER remote sensing data in Saindak deposit, Pakistan. *Geol. Rev.* **2022**, *68*, 2381–2395.

27. Tang, C.; Zhou, K.F.; Zhang, N.N.; Wang, S.S.; Zhou, S.G.; Du, Q.S.H.; Wang, X.L. Alteration Information Extraction Based on Integration and Fusion of Landsat-8 OLI and ASTER: A Case Study of Baogutu Porphyry Copper Deposit. *Bull. Geol. Sci. Tech.* **2018**, *37*, 211–217.
28. Wang, R.S.; Yang, S.M.; Yan, B.K. A review of mineral spectral identification methods and models with imaging spectrometer. *Remote Sens. Nat. Resour.* **2007**, *1*, 1–9.
29. Bai, L.Y.; Dai, J.J.; Wang, N.; Li, B.L.; Liu, Z.B.; Li, Z.J.; Chen, W. Remote sensing alteration information extraction and ore prospecting indication in Zhule-Mangla region of Tibet based on the GF-5 satellite. *Geol. China* **2022**, *1*, 1–18.
30. Wu, C.Y.; Dai, J.J.; Chen, W.; Jiang, B.; Wang, D.H.; Wang, C.L.; Wang, W.J.; Sun, H.Z.; Wang, Q.; Chen, W.; et al. Extraction of remote sensing alteration information and its ore prospecting indication in Sumochagan Obao fluorite mining area, Inner Mongolia. *Miner. Depos.* **2023**, *42*, 845–858.
31. Zhang, C.; Ye, F.W.; Xu, Q.J.; Liu, H.C.; Meng, S. Alteration information extraction of SASI hyperspectral images based on MTMF. *Geol. Rev.* **2015**, *61*, 428–429.
32. Hou, Z.Q.; Xie, Y.L.; Xu, W.Y.; Li, Y.Q.; Zhu, X.K.; Zaw, K.; Beaudoin, G.; Rui, Z.Y.; Huang, W.; Ciren, L. Yulong Deposit, Eastern Tibet: A High-Sulfidation Cu-Au Porphyry Copper Deposit in the Eastern Indo-Asian Collision Zone. *Int. Geol. Rev.* **2007**, *49*, 235–258.
33. Xie, X.P.; Bai, M.W.; Chen, Z.C.; Liu, W.B.; Xi, S.N. Remote sensing image interpretation and tectonic activity study of the active faults along the northeastern segment of the Longmenshan fault. *Remote Sens. Nat. Resour.* **2019**, *31*, 237–246.
34. Tian, S.F.; Zhan, Q. *Remote Sensing Geology*; Geology Press: Beijing, China, 2013.
35. Dai, J.J. Application of PALSAR and RADARSAT2 Quad-Polar Data to study of Geological Structure. *Geol. Prospect.* **2011**, *47*, 719–725.
36. Lian, C.Q.; Yao, F.J.; Feng, Z.M.; Yang, J.M.; Jia, X.X. Mineral Resources Prospecting by Synthetic Application of Multi-Source Data in the Shanyangba Area, Gansu, China. *Geoscience* **2022**, *36*, 1605–1612.
37. Bierwirth, P.; Huston, D.; Blewett, R. Hyperspectral Mapping of Mineral Assemblages Associated with Gold Mineralization in the Central Pilbara, Western Australia. *Econ. Geol.* **2002**, *97*, 819–826. [[CrossRef](#)]
38. Kruse, F.A.; Perry, S.L.; Caballero, A.O.D. District-level mineral survey using airborne hyperspectral data, Los Menucos, Argentina. *Ann. Geophys.* **2006**, *49*, 83–92.
39. Rockwell, B.W.; Cunningham, C.G.; Breit, G.N.; Rye, R.O. Spectroscopic Mapping of the White Horse Alunite Deposit, Marysvale Volcanic Field, Utah: Evidence of a Magmatic Component. *Econ. Geol.* **2006**, *101*, 1377–1395. [[CrossRef](#)]
40. Yan, B.K.; Dong, X.F.; Wang, Z.; Yang, S.M.; Yu, J.C.; Li, N.; Gan, F.P. Mineral information extraction technology by airborne hyperspectral remote sensing and its application progress: An example of mineralization belts of western China. *Geol. Surv. China* **2016**, *3*, 55–62.
41. Jiang, Q.; Dai, J.J.; Wang, D.H.; Tian, S.F. Application of optical remote sensing to identifying granite pegmatite lithium deposits. *Miner. Depos.* **2021**, *40*, 793–804.
42. Geng, X.X.; Yang, J.M.; Yao, F.J.; Yang, F.Q.; Liu, F.; Chai, F.M.; Zhang, Z.X. A study of Remote Sensing Prospecting Deposits Information of Abagong Iron Deposits in Altay region, Xinjiang. *Geol. Rev.* **2010**, *56*, 367–375.
43. Seltmann, R.; Porter, T.M.; Pirajno, F. Geodynamics and metallogeny of the central Eurasian porphyry and related epithermal mineral systems: A review. *J. Asian Earth Sci.* **2014**, *79*, 810–841. [[CrossRef](#)]
44. Sillitoe, R.H. Porphyry Copper Systems. *Econ. Geol.* **2010**, *105*, 3–41. [[CrossRef](#)]

Disclaimer/Publisher’s Note: The statements, opinions and data contained in all publications are solely those of the individual author(s) and contributor(s) and not of MDPI and/or the editor(s). MDPI and/or the editor(s) disclaim responsibility for any injury to people or property resulting from any ideas, methods, instructions or products referred to in the content.